16th World Conference on Earthquake, 16WCEE 2017

Santiago Chile, January 9th to 13th 2017

Paper N° 2588

Registration Code: S-T1464738789

FULL-SCALE EXPERIMENTAL ASSESSMENT OF STEEL-ENCASED BUCKLING RESTRAINED BRACES

M. Dehghani[1], R. Tremblay[2]

(1) Graduate Student, CGM Dept., Polytechnique Montreal Montreal, Canada, morteza.dehghani@polymtl.ca

(2) Professor, CGM Dept., Polytechnique Montreal Montreal, Canada, robert.tremblay@polymtl.ca

Abstract

Dissipation of seismic energy through large plastic deformations in ductile elements is a key approach to provide structural safety in strong earthquakes. Steel buckling-restrained braces (BRBs) offer significant energy dissipation capability by non-degrading plastic response of the internal steel core in tensile and compressive deformation cycles. Seismic performance of BRBs is affected by several factors such as the core-restrainer gap, the stiffness of the restraining system, and the interfacial friction between the core and the restrainer. This paper presents the results of 12 full-scale tests on BRB specimens made with an all-steel simple-to-fabricate restrainer jointed by high strength bolts. A simple hinge detail is also introduced at the brace ends to reduce the flexural demand on the framing components. The effects of interfacial friction between the core and the restrainer, gap size, loading history, bolt spacing, and local stiffness of the restraining mechanism are verified in these tests. Two practical pressure-sensitive UHMW polyethylene and PTFE tapes, and a graphite-based dry film lubricant are used as debonding material between the restrainer and the core. The influence of fast loading rates on axial resistance and low cycle fatigue life of BRB is examined through successive application of real-time seismic deformations histories. The performance of the brace member is also qualified under typical long-duration subduction inter-plate earthquakes. Internal restrainer thrust forces are evaluated using series of instrumented bolts. It is shown that insufficient strength can lead to significant strong-axis core buckling and subsequent loss of loading bearing capacity of BRB member in compression.

Keywords: Buckling-restrained braced frames; friction; debonding; seismic loading;

1 Introduction

Buckling-Restrained Braced Frames (BRBFs) have become a viable choice for seismic lateral force resisting systems in buildings and other types of structures. BRBFs are equipped with special brace members that play the fuse role by dissipating earthquake energy through predominantly axial plastic deformations in a stable manner. The buckling restrained brace (BRB) members are typically composed of a slender metallic element called core and an encasing system to prevent lateral buckling of the core. To ensure free relative sliding of the core and encasing, typically a small gap is left and a debonding material is used between these two parts. Since the core is prevented from buckling, it can be compressed far beyond yield capacity without strength degradation and this behaviour provides significant source of energy dissipating capacity. BRB technology was developed in the 1980's in Japan as a supplemental damping device for steel moment resisting frames [1]. Two decades later, this technology was adapted as a braced frame system in North America after experimental verification programs [2, 3]. The stiffness of the restrainer, the interface gap and friction between the core and the restrainer, and strain hardening of the core are the major parameters that control the behavior of a typically BRB member under large plastic strain cyclic loading. In reality, the force demand imposed on the restrainer components comes from a complex interaction between these variables. Traditionally, the buckling-restraining system is made of a concrete-filled steel tube and a soft and low-friction material is placed at the interface between the two materials to achieve free sliding response. As an alternative, the encasing can be fabricated entirely out of steel to eliminate time and efforts required for concrete casting and curing procedures. For such all-steel BRB members, the main challenge is to design a steel restraining system that provides a uniformly stiff lateral support for the core as it is typically achieved with a concrete-filled tube system. In a number of past experimental research projects on all-steel BRBs, premature failure has been observed due to insufficiency of the buckling restraining system [4, 5]. However, despite the importance of the subject, little attention has been given to developing proper and optimized design procedures for the restrainer member of steel-encased BRBs.

In this paper results of the experimental qualification of a BRB member system with a bolted fully-steel encasing are presented. The proposed patent-free BRB member is simple to fabricate and install. Key parameters affecting the seismic performance of the BRB member were investigated through twelve heavily-instrumented full-scale cyclic tests. In particular, the member performance is verified and compared with different restrainer-core interfacial conditions. The BRB specimens were tested in a planer load frame to investigate the flexural demand imposed by frame action. A simple end connection detail is introduced to limit that demand and its response is qualified under different loading conditions.

2 Test Program

2.1 BRB specimens

Twelve full-scale BRB specimens with nominally-identical cores were tested with the variables listed in Table 3. The core was flame-cut from ¾" (19.05 mm) thick plates conforming to CSA G40.21-350WT category 4 steel with minimum yield strength of 350 MPa. As shown in Fig. 1, the yielding segment (YS) of the BRB core is 150 mm wide by 3.0 meters long. The YS length approximately covers 50% of the workpoint-to-workpoint length of the brace member. The width of the core at the end is increased to 350 mm to preclude yielding outside of the YS and net section tension failure at the end bolted connections. Between the end bolted connections and the core YS, the wider core segment is stiffened by means of two flange plates to form I-sections. In this stiffened core segment, long-slotted holes are used to connect together the core and the restrainer system and accommodate the free relative movement between them. In the frame, the core is oriented such that weak axis buckling of the core occurs in the plane of the braced frame. The brace core is connected to the frame gusset plates using 2 pairs of angles. A short (38 mm) length is left between the ends of the angles and the stiffened core segments to create a low-strength plastic hinge for limiting in-plane bending moments induced in the brace as a result of the rotation of the core relative to the gusset plate assembly taking place when the frame laterally deforms [6]. Past research have shown that these in-plane bending moments can be damaging to the brace and other framing components [7, 8].

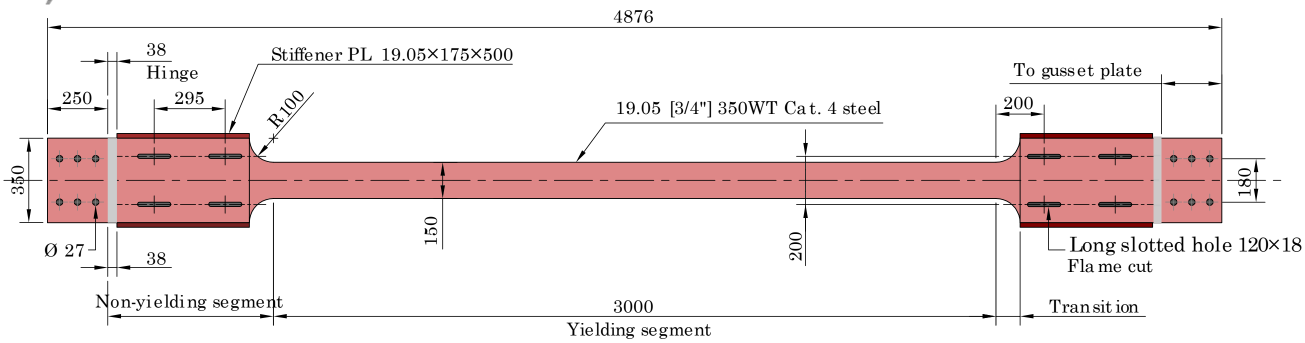

Fig. 1 – Geometry of the BRB core studied

Results from coupon tension tests of the core material at quasi-static rates of 1.0×10^{-6} s^{-1} are given in Table 1. Given the core YS section dimensions (19.05×150 mm) and the material yield strength, the nominal and actual axial yield resistances of the BRB core are 1000 and 1100 kN, respectively.

Table 1 – Average mechanical properties of core plate

Elastic Modulus (GPa)	**Upper Yield Stress** (MPa)	**Yield Stress** (MPa)	**Ultimate Tensile Stress (UTS)** (MPa)	**Strain at UTS** (%)	**Elongation on 200 mm gauge** (%)	**Reduction in area at fracture** (%)
210	412	385	509	16	28	60

The BRB restraining system consists of a pair of bolted built-up steel sections. These sections comprised of a flat plate and a HSS member (see Fig. 2). Two different restrainer designs, restrainers R1 and R2, were utilized in the experimental program. Restrainer R1 was proportioned to avoid global buckling of the brace member and resist the outward force demand imposed by the core undergoing two full-cycles at 0.04 storey drift angles. Given the geometry of the problem, the target drift angles correspond to nearly 4% axial elongation or shortening in the yielding segment of the BRB. A reduced target storey drift of 0.03 was considered for restrainer R2. As shown in Fig. 1, compared to restrainer R2, restrainer R1 was fabricated with a thicker HSS and thicker plates. It also required more closely spaced connecting bolts. Except for these differences, the two restrainer systems were identical. In both cases, the restrainer half-sections were bolted together using 15.7 mm (5/8”) high strength ASTM A325 bolts that were pre-tensioned to a minimum of 70% of the nominal tensile strength of the bolts (~85 kN). The bolts in the last two transversal bolt lines at the ends connect to the long-slotted holes in the non-yielding segment of the core to allow relative longitudinal movements between the restrainer system and the core (see Fig. 2c and d). These bolts were left in the snug-tight condition to minimize frictional resistance. The long-slotted holes were sized to allow for 4% elongation or shortening of the core YS. Longitudinal stoppers between the core and the restrainer were not used and both components were therefore free to slide with respect to each other. Out-of-plane (strong axis) buckling of the core YS is restrained by a pair of 47 mm wide shim plates placed on either side of the core YS and held in place by the longitudinal restrainer bolted connections. The side shims used in most of the specimens were cut from the same plate as the core, thus virtually having had the same thickness as the core. However, in few specimens, side shims were prepared from a generic 19.05 mm (¾”) plate which was slightly thicker than the core plates. Gaps were left on the four sides of the YS core to accommodate transverse core expansion due to Poisson’s effects under compression. The through-thickness gap was provided by thin steel sheets acting as spacers on top and/or bottom of the shim plates. The gap along the core sides was achieved by carefully placing the shim plates.

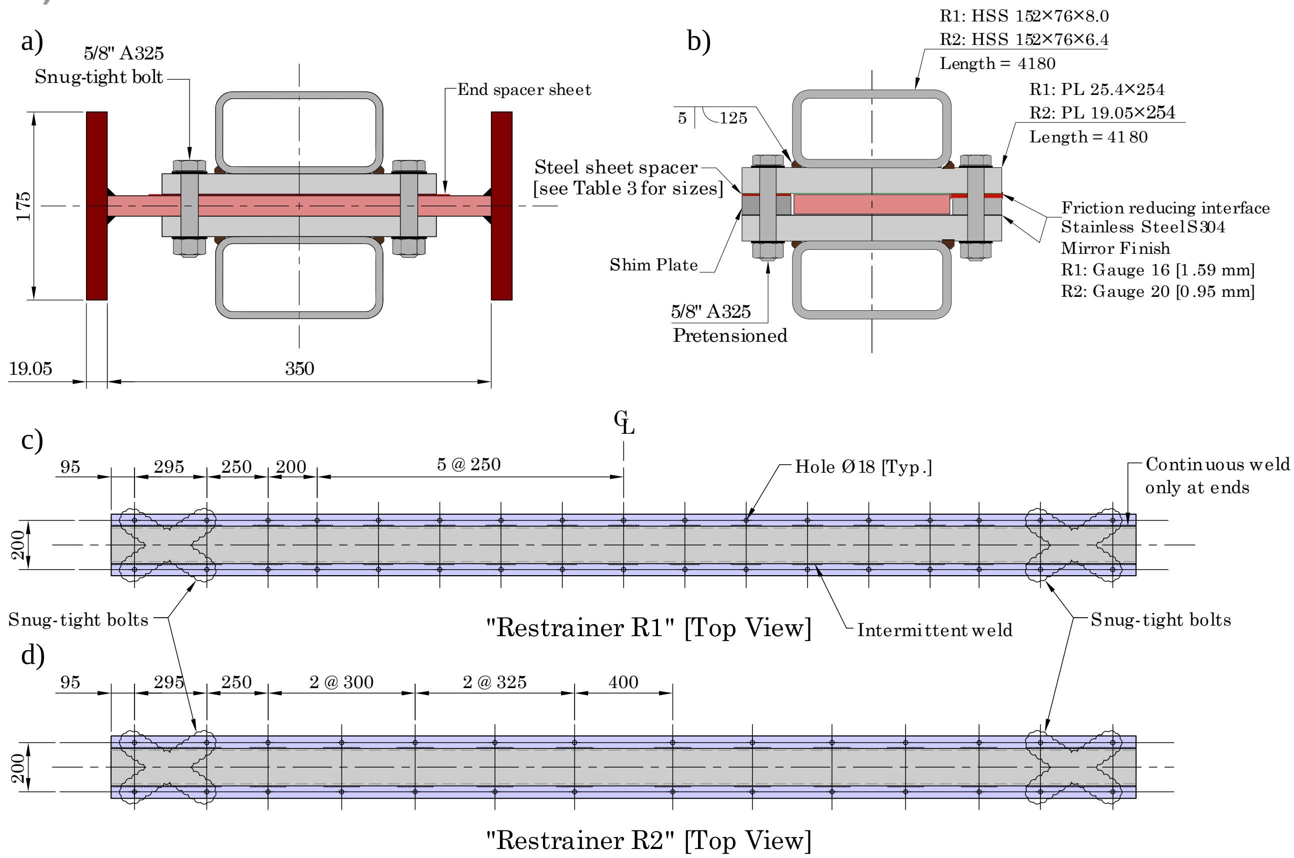

Fig. 2 – Typical cross-section view of the tested BRBs at: a) the stiffened area in non-yielding segment; and b) the yielding segment; bolt hole arrangement and welding scheme for restrainer: c) R1; and d) R2

2.2 Interfacial conditions

Frictional forces are generated as result of relative sliding between the core and the restrainer. The magnitude of these forces depends on the frictional characteristics of the interface of the two components and outward forces due to local core buckling. Excessive frictional forces can have adverse effects of the performance of BRBs [6]. This frictional resistance increases the energy dissipation capacity of the element at the cost of elevated demand on the force-controlled structural elements such as framing members and connections. High friction also causes non-uniform distribution of strain along the yielding segment of the core, which results in localization of plastic strains and, consequently, shortening of the fatigue life of the BRB member. The significance of frictional actions in BRBs are typically measured as the ratio of compressive to tensile resistances, $\beta = P_{max}/T_{max}$, at the instant of load reversal. Traditionally, in most available BRBFs, the core is debonded from restrainer by means of a low-friction material generally denoted as debonding layer. In this research, five interfacial conditions between the core and the restrainer were examined: 1) PTFE–SS, 2) UHMW–SS, 3) Graphite–Graphite, 4) BS– UHMW, and 5) BS-BS. BS stands for bare steel condition, meaning mill-finish quality without any additional debonding material. Properties of the debonding materials are presented in Table 2. PTFE (Polytetrafluoroethylene), also known as Teflon, is a smooth and flexible polymer that is widely popular in friction control applications. A notable PTFE structural engineering application is in sliding bridge bearings [9]. In this study, unfilled (virgin) PTFE was used against mirror-finished AISI Type 304 stainless steel (SS) with yield resistance of 215 MPa. The coefficient of friction for this interface is reported to be between 0.05 and 0.15 depending upon the normal stress and rate of sliding [10]. UHMW (Ultra-High-Molecular-Weight) polyethylene is also a polymer that has better wear resistance than PTFE but its coefficient of friction is relatively higher than PTFE (0.08 to 0.2). In this research, both PTFE and UHMW were supplied on the form of pressure-sensitive tapes which greatly facilitated their installation. The tapes were applied on the core plate except for Specimen 2 in which UHMW tape was placed on the restrainer face. Before the application, the steel surface was wire-brush cleaned, soap-washed, air-dried, and finally wiped down with a methyl-ethyl ketone solvent. This procedure was put in place to achieve maximum bond strength between tape and steel surfaces. The stainless steel was provided on the form of thin sheets (0.9 and 1.5 mm) placed against the restrainer flat plates, when applicable (see Fig. 4a). Graphite as a solid lubricant also provides an effective option for debonding purpose due to its high lubricity, low cost, endurance, and easy application. An industrial-grade dry film graphite lubricant (45% solids synthetic graphite) was roller-painted to the core and restrainer surfaces and then finished by latex glove covered-hands. The applied graphite coating typically becomes dry and solid in 24 hours and does not absorb dirt and dust, as typical liquid lubricant or gel greases would do, which could degrade the lubricity of the debonding layer.

Table 2 – Typical properties of the debonding materials verified in this study

Debonding Material	**Thickness of Applied Layer** (mm)	**Elastic Modulus** (GPa)	**Yield Resistance** (MPa)	**Coefficient of Friction** [(b)] (–)
PTFE	0.18 [(a)]	0.5	20	0.05–0.15
UHMW	0.33 [(a)]	0.8–1.5	19–23	0.08–0.2
Graphite	0.23	–	–	0.1–0.2

[(a)] total thickness of tape (backing (tape film) + adhesive)

[(b)] reported static coefficient of frictions for sliding against polished steel surface

2.3 Test setup and instrumentations

The overall view of the test setup is illustrated in Fig. 3. The setup represents a half span of a 9.0 by 4.0 m panel of a V braced bay. An approximately 6.0 m long BRB member was inserted in a load frame that consisted of a beam and a column. Lateral displacements were applied at the beam level with a pair of 1000 kN actuators. The load frame column was connected to the laboratory strong floor using a base-plate system with a hinge joint and the beam-to-column connection was a simple bolted double-angle joint with long-slotted holes in the angle legs connecting the beam web to accommodate the relative rotation between the beam and the column. Out-of-plane deformation of the load frame was restrained by friction-less sliding guides. As shown, the upper gusset plate was only connected to the beam bottom flange to minimize frame action. The clear distance between the gusset plate and the column face was set to prevent binding between the gusset plate vertical edge and the column flange up to 0.04 storey drift. The load frame was therefore expected to provide little lateral stiffness and resistance. This was verified by applying large amplitude cyclic deformations to the load frame without BRB. The measured maximum lateral resistance was around 10 kN, which represents less than 1% of the nominal yield resistance of the BRB members. The lower gusset plate was bolted directly to the laboratory strong floor. Both gusset plates were designed to remain completely elastic during the testing program. The BRB specimens were connected to the gusset plates long slot that were provided in the gusset plates (see Fig. 5b and c).

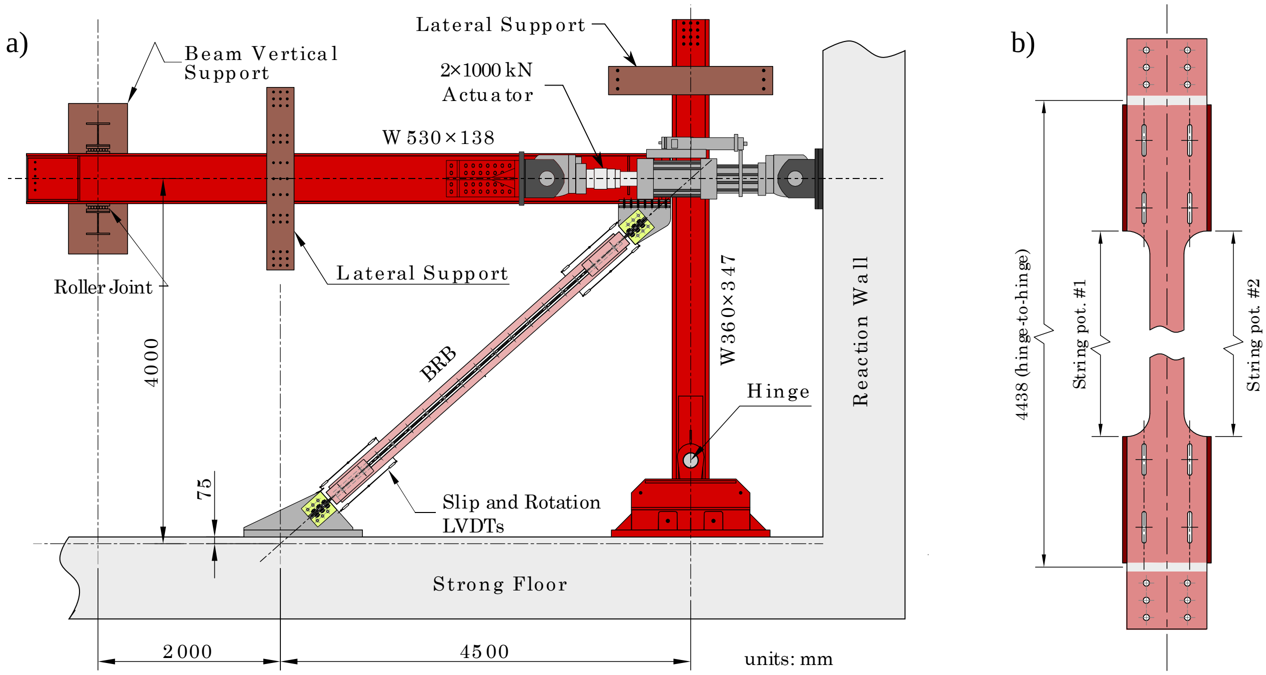

Fig. 3 – a) Vertical load frame layout; b) instrumentation to monitor displacement in the yielding segment of the specimens

At each brace end, pairs of LVDTs were placed between the gusset plates and the restrainer ends to track the longitudinal movement (sliding) of the restrainer. These sensors were also utilized to monitor relative in-plane rotations between the brace core and the gusset plates. Three-dimensional triangulation with string potentiometers was used to trace the spatial position of the middle of the brace and the bottom flange of the beam at the beam end. The spatial displacement data was then translated into relative in-plane and out-of-plane displacements at mid-length of the restrainer. Internal actions in the restrainer were estimated using the readings from 18 strain gauges installed at the brace extremities and mid-length. The location and position of these sensors are shown in Fig. 4b. Longitudinal distribution of axial frictional forces in the restrainer and in- and out-of-plane bending moment profiles along the specimen length could then be computed from these readings. Two identical restrainer R1 sets were used in the tests. In restrainer R1a, the extremity strain gauges were installed close to the snug-tight bolts where composite action between the two restrainer halves is limited. In restrainer R1b, the extremity strain gauges were installed along the first row of pre-tensioned bolts. In Specimens 9 to 11, half of the pre-tensioned bolts, i.e. 10 bolts, were instrumented to monitor the variation of tension load in the bolts along the core YS.

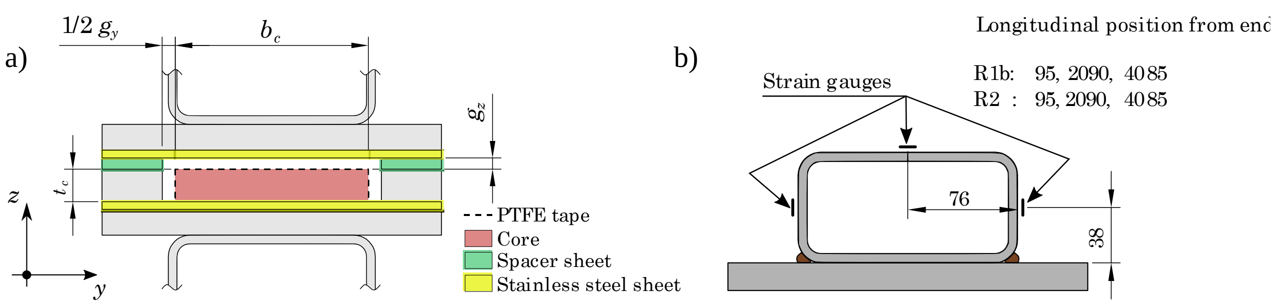

Fig. 4 – a) Schematic view of BRB cross-section (PTFE-Stainless steel interface condition shown); b) location and position of strain gauges to monitor internal actions in the BRB member

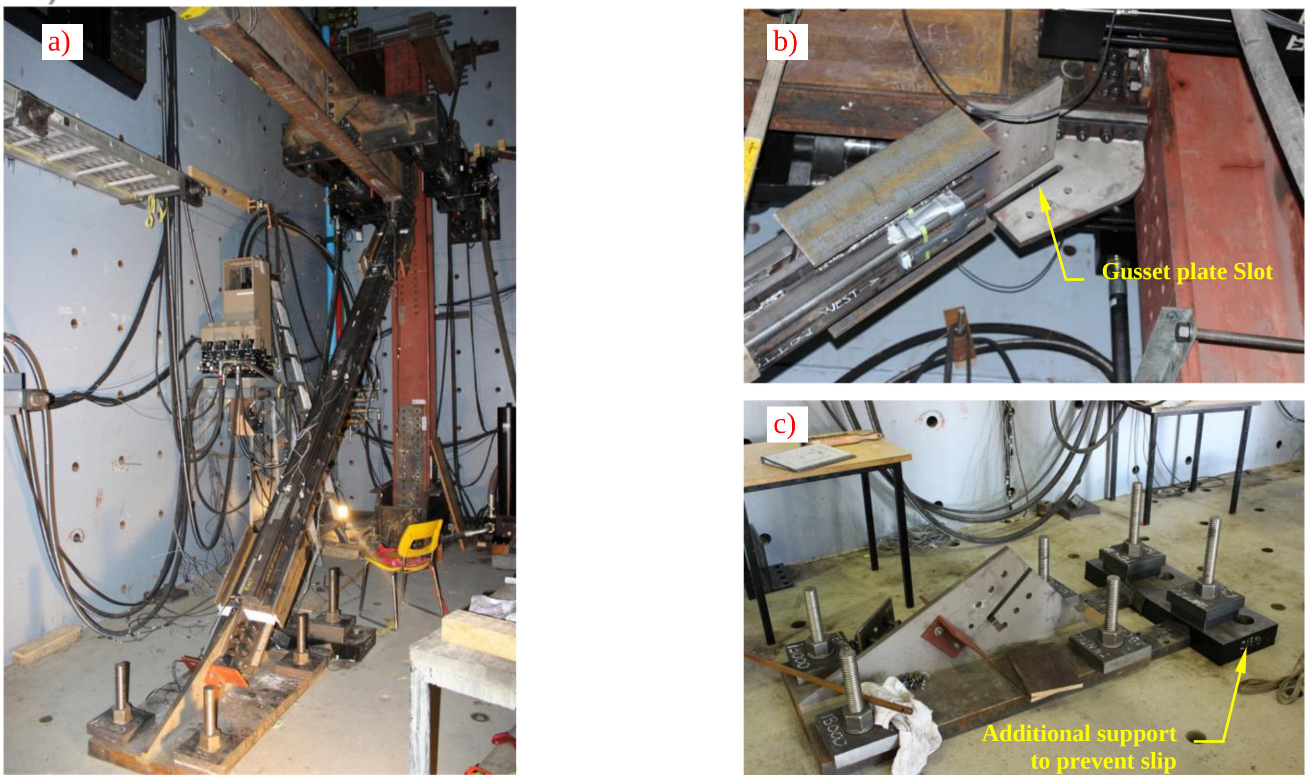

Fig. 5 – a) General view of the test setup (specimen 6); b) insertion of BRB into the upper gusset slot; and c) anchorage of lower gusset plate to the strong floor

2.4 Loading histories

Fig. 6 shows the three-stage cyclic (TSC) loading history expressed as equivalent uniform axial strain in the brace YS core. The first stage is a customized version of the AISC standard loading protocol for qualification of BRBs [11] for a storey design displacement inducing 1% core strain. As shown, it includes two additional cycles at three times the storey design displacement. The first stage finishes at a strain of 1%, which represents an average residual storey drift of 1% that is likely for code-compliant BRBFs subjected to design earthquake [12]. The second stage represents the demand from an aftershock earthquake and is centered about the residual displacement from the previous stage. The last excursion of the second stage simulates the response under pulse type motion that can be expected during a very strong aftershock. The last stage of the protocol consists of a fully-reversed constant-amplitude pattern that was repeated until BRB failure took place. It was applied to estimate the remaining low-cycle fatigue life of the BRB specimen after a shock-aftershock sequence. In the tests done with the TSC loading, storey displacement was applied using the axial deformation of the core YS as the feedback. The axial deformation of YS was monitored by the pair of string potentiometers shown in Fig. 3b. All loading stages of TSC were applied at a constant YS axial deformation rate of 0.75 mm/s, which corresponds to strain rate of 250×10^{-6} s^{-1} in the YS. This is 250 times faster than the rate at which the coupon tensile tests were conducted.

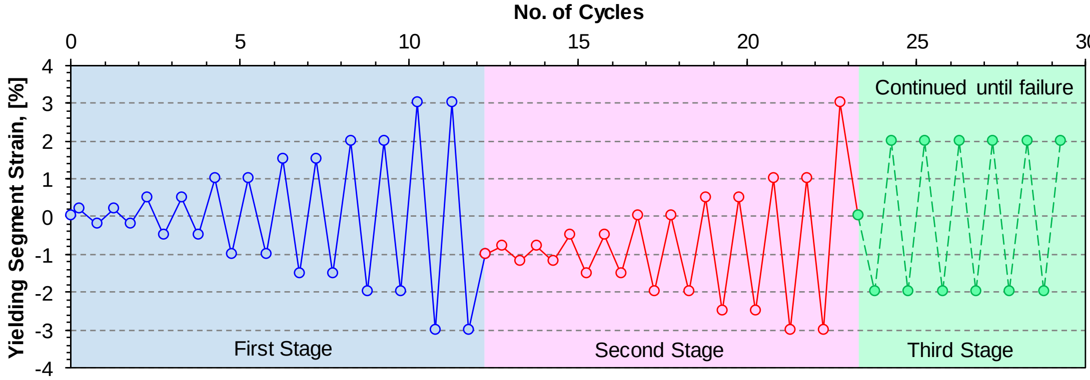

Fig. 6 – Three-stage cyclic (TSC) loading pattern

In addition to the three-stage cyclic loading history in Fig. 6, two seismic loading histories were also employed that represented the demand anticipated from two types of earthquake ground motions that are expected in southwest British Columbia (BC) along west coast of Canada: 1) Far-field intra-plate crustal earthquake; and 2) Subduction interface earthquake. Far-field intra-plate crustal ground motion records are typically free of rupture directivity effects and have normal strong motion duration. On the other hand, the subduction interface earthquakes generally have long duration of strong shaking which could promote failure mode associated to low cycle fatigue. The far-field (FF) signal was obtained from the response-history analysis of a 9-storey BRBF designed for Victoria, BC, under the NS component of the BRN record during the 1989 Loma Prieta earthquake. A scale factor of 1.5 was applied to the ground motion to match the site specific spectrum established for a 2% in 50 year probability of exceedance. The scaled record imposed storey drifts varying between −2.2 to 2.0% and cumulative inelastic ductility of 180 in the brace YS. The subduction interface (SI) signal is from the storey drift history at the top floor of a 5-storey BRBF subjected to the EW component of the ground motion recorded at the FSK005 station during the 2011 M9.0 Tohoku earthquake. The original signal was 300 s long. It was shortened to 150 s by removing the low amplitude cycles at the beginning and end of the signal. In the test with the FF and SI signals, the feedback from the actuators displacement was used as the control parameter.

2.5 Test matrix

The test matrix is given in Table 3. The first specimen served as dummy to verify the test set-up for quasi-static and real-time seismic loading histories. Specimens 2, 3, 4, and 6 were identical with the exception of the interfacial condition. They were all tested under the TSC loading history. The goal of this phase was to identify the interface condition that would lead to minimum frictional forces at the interface of the core and the restrainer. Specimen 6 with no debonding material represents a minimum cost BRB solution and the steel surfaces were left in the as-received condition. In Specimen 2, the steel of the restrainer flat plate was wire-brush cleaned before assembly. In the next round of testing program, the effect of gap size on the brace response indices was explored by comparing Specimens 4 and 5. The two specimens had identical specifications except that the through-thickness gap, g_z, was approximately doubled by using thicker sheet spacers. Specimens 7 and 8 were used to examine the behavior of the proposed BRBs under the seismic signals FF and SI, respectively. These two specimens had the same properties as Specimen 4. Specimens 9 and 10 were tested with the lighter restrainer R2 in order to verify simultaneous effects of a more flexible restrainer and tighter gap sizes. Specimen 11 is a replica of Specimen 4 except that larger through-thickness gap is specified and the restrainer bolt spacing is doubled. Specimen 12 was similar to Specimen 11 except that the gap g_z was same as in Specimen 5 and additional loosened bolts were placed between the pre-tensioned bolts to control out-of-plane buckling of the core. Specimens 9–12 were also used to compare the frictional response of the PTFE–SS and UHMW–SS interface conditions.

Table 3 – Test matrix

Specimen	Width, b_c [a] (mm)	Thickness, t_c [a] (mm)	Loading [b]	g_z [c] (mm)	g_y [d] (mm)	Debonding layer thick. [e] (mm)	Restrainer	S_x [f] (mm)	Interface condition [h]
1	150.90	19.01	TSC	1.44	8.45	0.36	R1a	250	PTFE–SS
2	151.21	19.01		1.44	9.61	0.66			BS–UHMW
3	150.26	19.05		1.40	9.97	0.46			Graphite–Graphite
4	151.39	19.00		1.45	7.04	0.36			PTFE–SS
5	150.43	18.96		3.35	7.99	0.36			PTFE–SS
6	150.23	19.05		1.41	10.02	–	R1b		BS–BS
7	150.28	18.92	FF	1.83	7.27	0.36	R1a		PTFE–SS
8	151.23	18.94	SI	1.81	6.27	0.36			PTFE–SS
9	150.12	18.92	TSC	1.08	4.68	0.36	R2	300	PTFE–SS
10	149.35	18.93		1.37	7.49	0.66			UHMW–SS
11	151.49	18.90		2.67	6.71	0.36	R1b	500	PTFE–SS
12	149.20	18.94		3.05	5.27	0.66		500 [g]	UHMW–SS

[a] average of measured values at 5 equally distance positions along the yielding segment
[b] TSC: Three-stage cyclic loading; FF: Far-field seismic loading; and SI: Subduction interface seismic loading.
[c] total through-thickness gap between core and restrainer (thickness of the debonding layer is not deducted).
[d] average measured total gap between core and side shim plates.
[e] thickness of debonding layer on each side of core.
[f] longitudinal distance between the restrainer pre-tensioned bolts (at ends of core YS for restrainer R2).
[h] core versus restrainer flat plate.
[g] loose bolts are added between each pre-tensioned bolt to prevent strong-axis buckling of core.

3 Experimental Results

Key response parameters measured in the tests are presented in Table 4. Values of maximum tensile and compressive core strains, ϵ^{+}_{max} and ϵ^{-}_{max}, and maximum core strain range $\Delta\epsilon$ sustained by the specimens are reported, together with the accumulated inelastic deformation (CID) up to failure, the maximum values of the force adjustment factors in tension and compression, ω_{max} and β_{max}, respectively, and failure description. For specimens subjected to the cyclic test (TSC loading history), values of the force adjustment factors after completing the 2% strain cycles corresponding to twice the design storey displacement, $\omega_{2\%}$ and $\beta_{2\%}$, are also given as those would typically be used in design. After testing, the specimens were opened and inspected for failure location and buckling wave lengths. The test on Specimen 1 confirmed the adequacy of the test setup. However, it was observed that considerable relative displacements took place in the beam-to-column bolted connection and larger than anticipated storey drifts (beam lateral displacements) had to be applied to impose the intended strain demands on the brace core YS. Similar response was observed in all subsequent tests. Due to the higher deformation rate in the full-scale brace tests, the yield stress of the core material showed ~15% increase with respect to the coupon tests. Specimen 1 was also use to fine tune the control scheme in the real-time seismic loading histories. Damage to the clip angles due to bolt bearing developed during the tests and the clip angles had to be replaced three times in the test program. Hysteresis response of some specimen is shown in Fig. 9.

Specimens 2, 3, and 4 showed similar behavior. They all sustained the first and second stages of the TSC loading and failed during the 3rd loading stage. Failure occurred in tension without any noticeable damage on the restrainer parts. Among the three specimens, as shown in the table, the measured force adjustment factors are comparable. However, Specimen 4 with the PTFE-SS interface sustained the largest number of cycles and exhibited the highest CID value. In testing Specimens 2, vertical edge of top gusset plate become in contact with the column flange at the end of +3% strain cycles and as a result the flexural stiffness of the frame column was engaged. This explains the gradual change in the hardening slope toward the end of largest tensile excursion in the hysteresis response of Specimen 2 (see Fig. 9a).

Specimen 6 with steel–steel interfacial condition, showed significantly higher tensile and compressive resistances (ω = 1.61 and β = 1.47) in comparison with the previous tests. In the middle of the 2nd loading stage, the compressive resistance became so high that the capacity of the actuators (2000 kN) was exhausted and test had to be stopped. Examination of the specimen after the test showed the bolts connecting the core and the restrainer in the slotted holes at the brace ends had imposed significant inelastic bearing deformations to the 0.76 mm thick spacer steel sheet with standard size holes. This spacer sheet was placed between the core and the restrainer in the non-yielding core segments (see Figs. 7a–b). This observation suggested that because of the higher friction of the BS surface condition, the end spacer sheets restrained the longitudinal movement of the core relative to the restrainer, which contributed to the large axial resistance exhibited by the specimen. When the test was halted, necking had formed in the core YS (Fig. 7a) and the specimen was therefore near failure. It had then reached a CID of 323, which exceeds the minimum value of 200 specified in the AISC qualification requirement for BRB members. The maximum compressive strength adjustment factor of this specimen at +/−2% strain cycles, $\beta_{2\%}$, was 1.25 which is less than the maximum value permitted by the AISC qualification standard, i.e. $\beta \leq 1.3$.

Specimen 7 was subjected to far-field displacement history. This specimen showed excellent performance and the complete history had to be repeated 13 times before fracture of the core YS occurs. During the first 10 passes of this loading history, displacements were applied at real-time rate. The hydraulic power supply of the actuators reached its flow capacity due to the fast rate large horizontal displacements that had to be applied and the target YS strain could not be fully reached. As a result, the actual CID was reduced from 180 to 120 during these loading passes. In the last three passes, 11 to 13, the loading rate was reduced by a factor of 10 so that the target core YS strain could be fully reached. In total, the yielding segment of this specimen sustained a CID value more than 1600 before fracture. Specimens 7 and 4 were identical and the similitudes between the CID and force adjustment factors measured in the two tests suggest that cyclic qualification protocols can predict well the BRB fracture life and maximum expected forces under actual seismic demand. For specimen 8, the same reduced loading rate was used so that the YS strain history induced by the subduction interface earthquake could be fully imposed. The specimen sustained without failure 9 passes of this long duration seismic history. It was then subjected to 0–0.03 YS strain cycles and failure occurred in the 30th cycle after accumulated inelastic deformations of 3700. Unlike the other previously tested specimens which fractured inside the YS, failure of Specimen 8 occurred at the transition area of the core. In this test, the plastic hinges at the brace ends were subjected to numerous cycles of high axial loads and rotations. They performed very well without any sign of damage or distortion. Specimens 9 and 10 were tested using restrainer R2. This lighter restrainer was designed for two cycles of 0.03 rad. storey drift angle and had lower flexural stiffness and wider longitudinal bolt spacing in the core YS. Relatively tighter through-thickness gap was specified for these specimens. Both specimens survived successfully the 1st and 2nd stages of the TSC loading and failed in the third stage. Specimens 9 could sustain two cycles more than Specimen 10, indicating that the PTFE-SS interface may lead to slightly longer fracture life compared to the UHMW–SS condition. In these two experiments, no visible distortion was observed in the restrainer and the strain gauge readings confirmed that the restrainers behaved elastically. Comparison between Specimens 4 and 9 shows that the restrainer size and number of bolts could be optimized by using properly sized through-thickness gap without compromising the performance. Specimen 11 and 12 were tested with wider-than-required restrainer bolt spacing to promote undesirable failure modes. Specimen 11 with 500 mm bolt spacing sustained the first loading stage without failure. However, at the end of this stage, the side shim plates were significantly bent and pushed out of the restrainer at two opposite end sides of the specimen, revealing buckling of the core about its strong axis (Fig. 8a). Application of additional cycles of deformation cycles resulted in fracture of the bolts in double shear due to the lateral thrust forces imposed by core strong axis buckling. Core buckling became more pronounced with loss of brace axial compressive strength. The restrainer remained essentially elastic as the damage concentrated in the side shim plates and the core YS (Fig. 8b). In Specimen 12, out-of-plane (strong axis) buckling of the core was precluded by adding non-tightened bolts between the pretensioned bolts spaced 500 mm c/c. The non-tightened bolts were entirely loose and did not contribute to prevent core weak axis buckling. As expected, Specimen 12 sustained the first loading stage without strong axis buckling of the core YS. In the last compressive cycle of the 2nd loading stage with $\Delta\epsilon$ = 4%, two pre-tensioned restrainer bolts fractured in tension due to core weak axis buckling response. Three additional pre-tensioned bolts fractured in the same manner when the load was reversed to compression after imposing a

3% tensile YS strain. The specimen eventually lost its compressive resistance due to excessive core buckling. When the specimen was unloaded, permanent bending deformation of the restrainer was still appreciable. The deformed shape of the buckled core after removal of the restrainer is shown in Fig. 8c.

Table 4 – Summary of test results

Specimen	ϵ^{+}_{max} (%)	ϵ^{-}_{max} (%)	$\Delta\epsilon$ (%)	CID † (–)	ω_{max} (–)	β_{max} (–)	$\omega_{2\%}$ (–)	$\beta_{2\%}$ (–)	Description of failure
1	2.9	2.9	5.8	1623	1.46	1.15	1.35	1.11	specimen used to check the setup, no failure
2				672	1.48	1.16	1.37	1.11	failure in 8th cycle of 3rd stage
3				965	1.45	1.16	1.36	1.11	failure in 17th cycle of 3rd stage
4				1228	1.46	1.15	1.37	1.12	failure in 23rd cycle of 3rd stage
5	3.0	3.0	6.0	765	1.49	1.14	1.40	1.09	failure in 11th cycle of 3rd stage
6				323	1.61	1.47	1.43	1.25	test stopped at the middle of 2nd stage due to actuators force capacity
7	1.5 [2.0] *	2.2 [2.3] *	2.3 [3.6] *	1657	1.42	1.14	–	–	tensile fracture in the 13rd pass
8	2.6 [3.2] **	1.65 [0.0] **	2.2 [3.3] **	3707	1.39	1.13	–	–	no failure after 9 passes; failure in subsequent 0–3% YS strain loading (30th cycle)
9				859	1.45	1.19	1.39	1.12	failure in 14th cycle of 3rd stage
10				795	1.43	1.17	1.40	1.13	failure in 12th cycle of 3rd stage
11	3.0	3.0	6.0	412	1.47	1.08	1.43	1.08	strong-axis buckling of the core producing bolt shear failure and fracture of side shims in the 2nd stage
12				421	1.43	1.19	1.37	1.14	bolt tension failure resulting in weak-axis core buckling in the 2nd stage

† total cumulative inelastic ductility (sum of plastic deformation increments normalized by core yield displacement) up to failure

* number in brackets are from slow rate loading

** number in bracket is from low cycle fatigue testing performed after seismic loading test

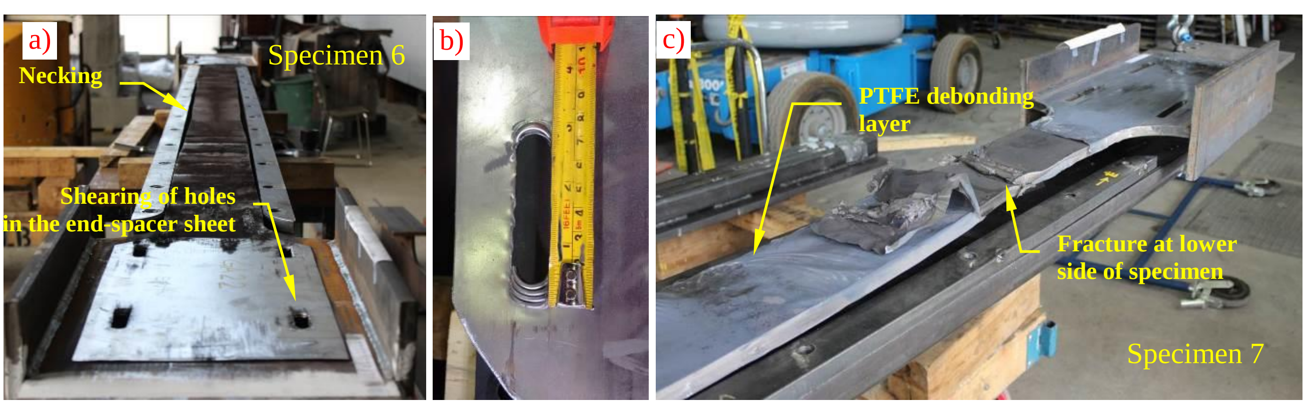

Fig. 7 – a) Deformation shape of core at the end of test of specimen 6; b) Shearing of standard hole in end-spacer sheet of specimen 6; and c) Fractured core of Specimen 7 under FF seismic loading

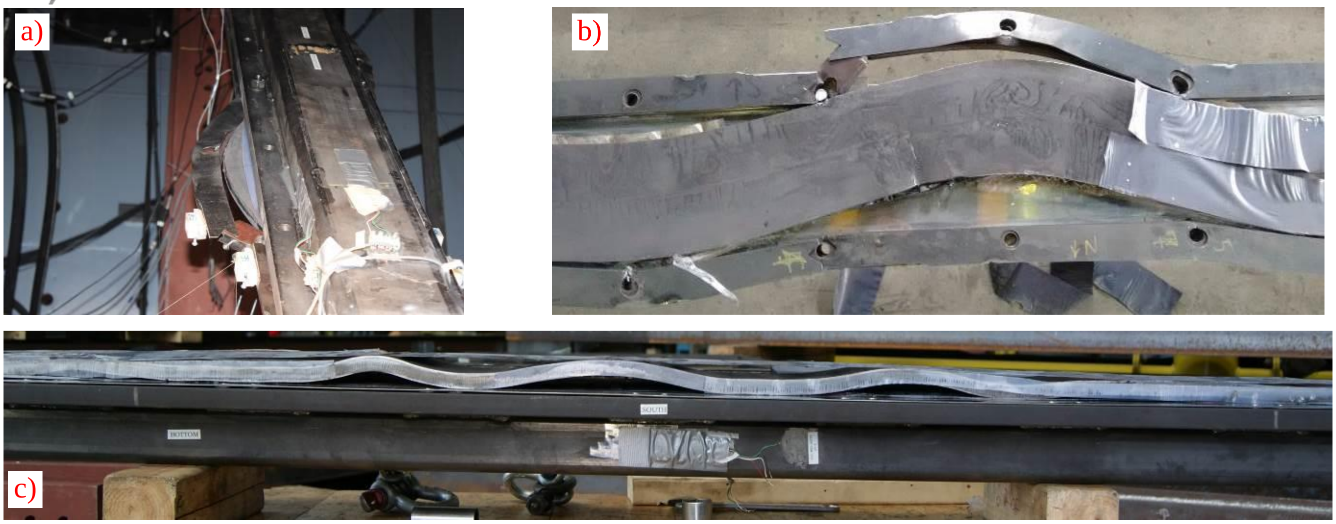

Fig. 8 – a) and b) Out-of- plane (strong axis) buckling of the core in Specimen 11; c) In -plane (weak axis) buckling of the core in Specimen 12.

In all tests on specimens with the PTFE and UHMW tapes, post-experiment investigation showed that both materials had good adhesive performance as they detached from the core surfaces only in a few spots. In some cases, the tapes broke locally due to excessive wear or tensile stresses. When subjected to the same conditions, the PTFE film performed slightly better than the UHMW one. Results from Specimens 4, 5 and 9 can be compared to examine the effect of through-thickness gap size. Specimen 4 with an intermediate (1.5 mm) gap exhibited a longer fracture life than Specimens 5 with 3.1 mm gap. Specimen 9 with ~1.0 mm gap performed very similar to Specimen 4 while it had a 20% lighter restrainer and less number of pretensioned bolts.

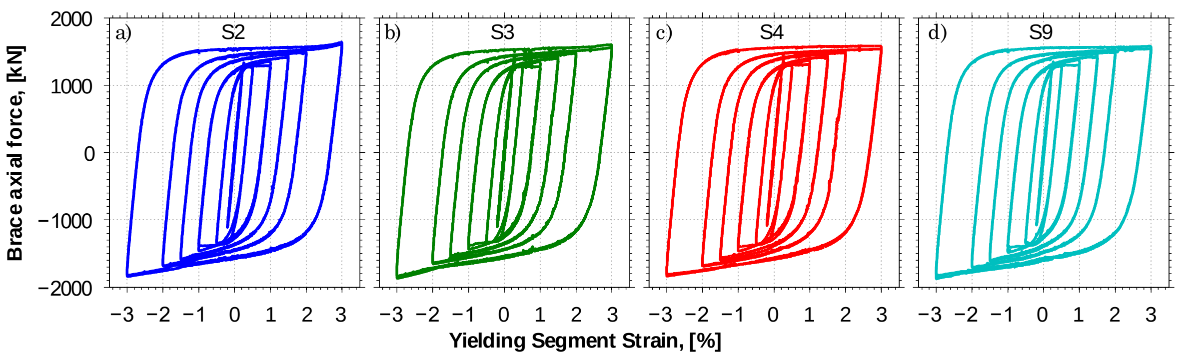

Fig. 9 – Hysteresis response of Specimen 2, 3, 4 and 9 in the first stage of TSC loading.

4 Conclusions

Full-scale buckling-restrained braces with bolted steel buckling restraining system were tested and the results were presented. Effects of parameters such as interface conditions, gap sizes, restrainer stiffness and loading conditions were evaluated and various types of failure mechanisms were observed. In general, the tested BRBs showed stable inelastic cyclic response and high cumulative ductility capacities varying from 320 to 3700 depending on the test parameters. The BRB system tested showed excellent performance under seismic loading conditions and exhibited significant post-earthquake ductility capacity. The tests showed the PTFE-stainless steel interface condition was very effective in reducing longitudinal frictional forces and achieving long fracture life. The results showed that proper gap size that, allows for transverse expansion while minimizing core buckling amplitude, is necessary to develop optimal fatigue life response. Core buckling about its strong and weak axes are possible failure mechanisms when insufficient restraining is provided.

Acknowledgements

Funding for this project was provided by the Natural Sciences and Engineering Research Council (NSERC) of Canada. The scholarship awarded to the first author by the Structural Steel Education Foundation of the Canadian Institute of Steel Construction is acknowledged. The core plate material was supplied by Canam-Bridges in Quebec City, Goodco Z-Tech Inc. in Laval, QC, donated the stainless steel sheets, and the specimens were graciously fabricated by Lainco Inc. from Terrebonne, QC.

References

[1] Watanabe A, Hitomi Y, Saeki E, Wada A, Fujimoto M (1988): Properties of brace encased in buckling-restraining concrete and steel tube. *The 9th World Conference on Earthquake Engineering*, Tokyo-Kyoto, Japan.

[2] Tremblay R, Degrange G, Blouin J (1999): Seismic Rehabilitation of a Four-Storey Building with a Stiffened Bracing System. *8th Canadian Conference on Earthquake Engineering*, Vancouver, BC, Canada.

[3] Black C, Makris N, Aiken I (2004): Component Testing, Seismic Evaluation and Characterization of Buckling-Restrained Braces. *Journal of Structural Engineering*, **130** (6), 880-894.

[4] Eryaşar ME, Topkaya C (2010): An experimental study on steel-encased buckling-restrained brace hysteretic dampers. *Earthquake Engineering & Structural Dynamics*, **39** (5), 561-581.

[5] D'Aniello M, Della Corte G, Mazzolani F (2009): "All-steel" buckling-restrained braces for seismic upgrading of existing reinforced concrete buildings. *The 6th International Conference on Behaviour of Steel Structures in Seismic Areas - STESSA (2009)*, Philadelphia, Pennsylvania.

[6] Tremblay R, Bolduc P, Neville R, DeVall R (2006): Seismic testing and performance of buckling-restrained bracing systems. *Canadian Journal of Civil Engineering*, **33** (2), 183-198.

[7] Takeuchi T, Ozaki H, Matsui R, Sutcu F (2014): Out-of-plane stability of buckling-restrained braces including moment transfer capacity. *Earthquake Engineering & Structural Dynamics*, **43** (6), 851-869.

[8] López WA, Gwie DS, Saunders CM, Lauck TW (2002): Lessons Learned From Large-Scale Tests of Unbonded Braced Frame Subassemblages. *The 71st annual convention of SEAOC*, Sacramento, CA.

[9] Dolce M, Cardone D, Croatto F (2005): Frictional Behavior of Steel-PTFE Interfaces for Seismic Isolation. *Bulletin of Earthquake Engineering*, **3** (1), 75-99.

[10] Bondonet G, Filiatrault A (1997): Frictional Response of PTFE Sliding Bearings at High Frequencies. *Journal of Bridge Engineering*, **2** (4), 139-148.

[11] AISC (2010): Seismic Provisions for Structural Steel Buildings (ANSI/AISC 341-10). American Institute of Steel Construction, Inc: Chicago, IL.

[12] Erochko J, Christopoulos C, Tremblay R, Choi H (2011): Residual Drift Response of SMRFs and BRB Frames in Steel Buildings Designed according to ASCE 7-05. *Journal of Structural Engineering*, **137** (5), 589-599.